Permanent Magnet Axial Section Shaping Optimization Surface-mounted Permanent Magnet Synchronous Motor

Shengnan Wu, *Member*, *IEEE*, Qifeng Zhao, and Wenming Tong, *Member*, *IEEE*

***Abstract*—In this paper, a new type of harmonic injection permanent magnet shape optimization method is proposed to suppress the torque ripple of surface-mounted permanent magnet synchronous motor. The sinusoidal waveform shaping of the axial section of the permanent magnet is added with the third harmonic shaping, and the sine wave and the third harmonic are derived. The optimal ratio is 6:1. The permanent magnet no shaping, sinusoidal shaping and sinusoidal combined third harmonic shaping are compared. The results show that the sinusoidal combined third harmonic shaping design can effectively suppress the torque ripple of the surface mounted permanent magnet synchronous motor and obtain a relatively large output torque. At the same time, a method of using permanent magnet segmentation to approximately equivalently replace sine combined with third harmonic shaping design is proposed, which effectively saves the manufacturing cost of permanent magnets and provides design and research ideas for more economical and effective optimization of surface-mounted permanent magnet motors.**

***Index Terms*—Permanent Magnet Synchronous Motor, Harmonic Injection, Torque Ripple, Segmented Magnet.**

I. INTRODUCTION

COMPARED with the built-in permanent magnet motor, the surface-mounted permanent magnet synchronous motor has the advantages of simple control, simple structure and small torque ripple. The surface-mounted permanent magnet motor is usually selected as the driving motor for industrial robots. Torque ripple is very important for high-quality servo motors that need to smooth speed and position adjustment. Especially at low speeds, the influence of torque ripple may be dominant, so the torque ripple of the motor must be minimized. Moreover, in order not to affect the other performance of the motor, the influence on the average output torque of the motor should be avoided while reducing the torque ripple.

In Reference [1], proposed an asymmetric magnet shape optimization analysis method for surface-mounted permanent magnet motors based on Schwarz-Christoffel mapping. The permanent magnet is divided into finite elements, combined with genetic algorithm optimization, significantly improves the cogging torque and torque ripple of surface mounted permanent magnet motor. In Reference [2], studied the pole tilt design and summarized the best pole tilt angle, which effectively reduced the torque ripple without causing a great impact on the output torque of the motor. In Reference [3], studied the method of drilling holes on the rotor surface, and determined the optimal number and size of holes by sensitivity analysis, which reduced the torque ripple without reducing the torque ripple of the motor. In Reference [4], in order to reduce the torque ripple of axial flux motors, discretely divided the permanent magnet into blocks to optimize the back electromotive force waveform, and proposed an analysis method to calculate the 3d model based on the 2d model to reduce the calculation time. In Reference [5], proposed a new magnetic field distribution analysis model of non-uniform particle shape to optimize the shape of permanent magnet and reduce motor torque ripple and core loss. In Reference [6], set reluctance slots at both ends of the rotor pole to optimize the air gap magnetic density waveform. Experiments show that this method has a good suppression effect on high-speed permanent magnet motor torque ripple, but the impact of this method on the output torque is not analyzed. In Reference [7], the magnetic bridge and stator teeth of the interior permanent magnet motor are used as research variables, and the rotor is slotted. The torque ripple is optimized by combining the second-order Kriging model and NSGA-II genetic algorithm. In Reference [8], it is proposed to use ferrite permanent magnets to replace part of NdFeB permanent magnets as magnetic poles to improve the air gap flux density waveform, and use Kriging model combined with genetic algorithm for further optimization. In Reference [9], the low torque ripple and high electromagnetic torque of the surface mounted permanent magnet motor are realized by using the permanent magnet segmented bias combined with the Halbach array magnetization. In Reference [10], taking the shape of permanent magnet and the magnetization angle of permanent magnet as the research object, the best permanent magnet structure is selected by Taguchi method, which can reduce the torque ripple of surface mounted permanent magnet motor and reduce the vibration noise of motor.

Many scholars have carried out a lot of analysis and research on reducing the torque ripple of surface-mounted permanent

Manuscript received December 26, 2022; revised February 04, 2023; accepted March 22, 2023. Date of publication December 25, 2023. Date of current version June 12, 2023.

This work was supported by the National Natural Science Funds of China No. 51907129 and Technology program of Liaoning province No. 2021-MS-236. (*Corresponding Author*: *Wenming Tong*)

Shengnan Wu, Qifeng Zhao and Wenming Tong are with the School of Electrical Engineering, Shenyang University of Technology, Shengyang 110870, China (e-mail: imwushengnan@163.com, 851592611@qq.com, twm822@126.com).

Digital Object Identifier 10.30941/CESTEMS.2023.00036

2096-3564 © 2023 CES

magnet motors. Each method has advantages and disadvantages. The common problem occurs while reducing the torque ripple. The average output torque of the motor will be greatly affected and cannot meet the requirements of practical applications. Based on the calculation formula of back electromotive force and output power of surface-mounted permanent magnet motor, this paper calculates and deduces the optimal ratio of sine wave and third harmonic shaping of permanent magnet axial section, and compares the back electromotive force waveform, torque ripple and average output torque. At the same time, from the point of view of saving manufacturing cost, the discrete segmentation of permanent magnet is approximated as sine wave and third harmonic shaping, and the finite element calculation is carried out for comparative analysis.

II. Permanent Magnet Synchronous Motor Structure

In order to study the influence of permanent magnet axial section shaping on torque characteristics, this paper takes two 20-pole 18-slot (20P18S) and 16-pole 18-slot (16P18S) surface-mounted permanent magnet motors with fractional-slot concentrated windings as examples. The two motor models are shown in Fig. 1, and the structural parameters of the motor are given in Table I.

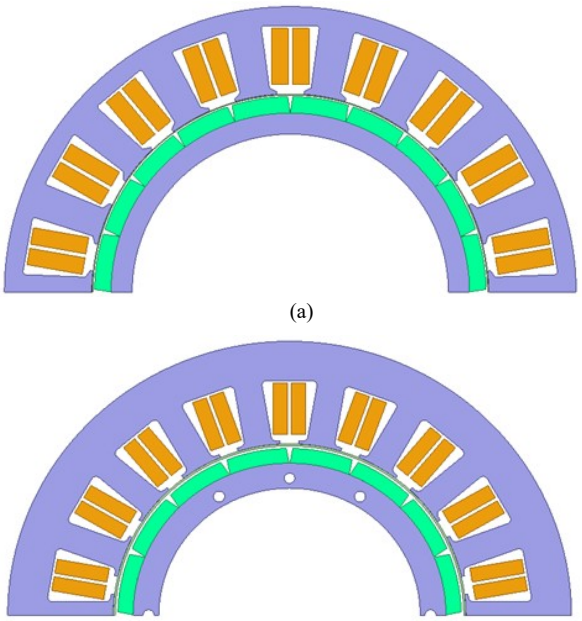

(a)

(b)

Fig. 1. Model structure of SPMSM. (a) 20P18S. (b) 16P18S.

III. Theoretical Analysis of Harmonic Injection Shaping Design

If the input current is a sine wave, ignoring the high-order harmonics of the input current, the high-order harmonics of the back electromotive force are the main factors causing torque ripple. In Reference [11], it is proposed that if there is a third harmonic component in the three-phase symmetrical AC winding, no matter how the phase winding is connected, there will be no time component in the induced line voltage in the star or triangular winding. Through this theory, the shape of the permanent magnet injected with the third harmonic on the basis of the sine wave can be designed. To simplify the calculation, the following procedures are at the

The derivation is carried out under the condition that the arc coefficient is 1.

In Reference [12], the no-load back electromotive force(EMF) of the motor is proposed

$$E = 4.44\ K_{dp}\ fN\Phi \tag{1}$$

where K_{dp} is the winding coefficient, f is the motor frequency, N is the number of conductors per pole per phase, per pole flux

$$\Phi = B_r S = B_r m l_{(\theta)} \tag{2}$$

where B_r is the air gap flux density, m is the width of permanent magnet, $l_{(\theta)}$ is the axial length function of permanent magnet.

Arranged from eq.(1) and (2), there is

$$E = 4.44 K_{dp} f N B_r m l_{(\theta)} \tag{3}$$

It can be seen from eq.(3) that the back electromotive force waveform is completely consistent with the function waveform of the effective length of the permanent magnet. If the length of the permanent magnet is a sine function, the back electromotive force waveform corresponds to a sine wave. The length function of sinusoidal permanent magnet is

$$l_{(\theta)} = l_a \sin(p\theta) \tag{4}$$

where l_a is the maximum axial length, p is the motor pole pairs, θ is the rotor rotation angle.

In reference [13], the total instantaneous electromagnetic torque expression of the permanent magnet motor is as follows

$$T_{em} = \frac{E_a I_a + E_b I_b + E_c I_c}{\Omega} \tag{5}$$

where E_a, E_b, E_c is the three-phase back EMF, I_a, I_b, I_c is the phase current, Ω is the angular velocity.

It can be obtained from eq. (3) and (5) that

$$T_{em} = \frac{3E_1 I_1}{2\Omega} = \frac{3I_1}{2} \cdot \frac{4.44 K_{dp} f N B_r m l_a}{\Omega} \tag{6}$$

When the permanent magnet is sinusoidal plus third harmonic shaping, the permanent magnet length expression is

$$l_{(\theta)} = l_b[\sin(p\theta) + x\sin(3p\theta)] \tag{7}$$

Since the overall structure of the motor cannot be affected,

TABLE I
Motor Parameters of SPMSM

Parameter	20P18S	16P18S
Rated power (kW)	0.15	0.075
Rated current (A)	14.3	6.9
Rated speed (rpm)	100	100
Stator outer diameter (mm)	208	178
Rotor cooling diameter (mm)	142.4	111.4
Rotor inner diameter (mm)	115	108.4
Axial length (mm)	23	22
Number of slot	18	18
Number of pole	20	16
Number of conductors per slot	46	30
Stator tooth width (mm)	11.8	8.8
Pole embrace	0.92	0.9
Permanent magnet thickness (mm)	5	4.8

the maximum length of the permanent magnet cannot be changed. Therefore, to determine the sine and third harmonic permanent magnet maximum position, when the absolute value of eq. (7) is 0, the maximum length position of the permanent magnet is

$$\cos(p\theta)=(\frac{9x-1}{12x})^{\frac{1}{2}} \tag{8}$$

The maximum length of permanent magnet is

$$l_{\max}=l_b 8x(\frac{1+3x}{12x})^{\frac{3}{2}} \tag{9}$$

The phase back EMF and electromagnetic torque of the sine and third harmonic shaping permanent magnet can be obtained by the formula

$$E=4.44K_{dp}fNB_r ml_b[\sin(p\theta)+x\sin(3p\theta)] \tag{10}$$

In order to obtain the maximum electromagnetic torque, the conditional extremum is obtained by using the method of substitution elimination under the condition of eq. (9)

$$\frac{dT_m}{d(x)}=0 \tag{11}$$

From the above formula can be derived

$$x=\frac{1}{6} \tag{12}$$

$$l_b\approx 1.155l_{\max} \tag{13}$$

Therefore, the optimal ratio of sine wave to third harmonic is 1:6, and the axial length expression of sine plus third harmonic permanent magnet is

$$l_{(\theta)}=1.155l_{\max}[\sin(p\theta)+\frac{1}{6}\sin(3p\theta)] \tag{14}$$

IV. Finite Element Simulation

In order to verify the analytical derivation process, a three-dimensional model is established for finite element analysis. The motor rotor structure model is shown in Fig. 2, Fig. 2(a) is the original model, Fig. 2(b) is the permanent magnet sinusoidal shaping(Sine Model), and Fig. 2(c) is the permanent magnet sinusoidal plus third harmonic shaping(Sine+3rd Model). Each permanent magnet is formed by splicing two shaping poles of equal size to ensure the symmetry of the air gap magnetic field without generating additional unbalanced magnetic pull.

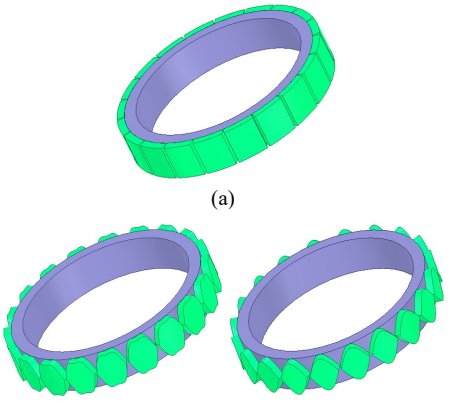

(a) (b) (c)

Fig. 2. Design of three different permanent magnet shapes. (a) Original model. (b) Sine Model. (c) Sine+3rd Model.

Compared with the original permanent magnet, the volume of the sinusoidal shaped permanent magnet decreases a lot, which will have a great influence on the average output torque of the motor in theory. After adding the third harmonic, the volume of the permanent magnet increases, which reduces the influence on the average output torque, and the increased third harmonic will not produce additional torque ripple.

The air gap magnetic density clouds of different permanent magnet shapes of the two motors are shown in Fig. 3 and Fig. 4. It can be seen that as the shape of the permanent magnet changes, the air gap flux density also changes accordingly, from the initial rectangle to the sine shape and the sine plus third harmonic shape.

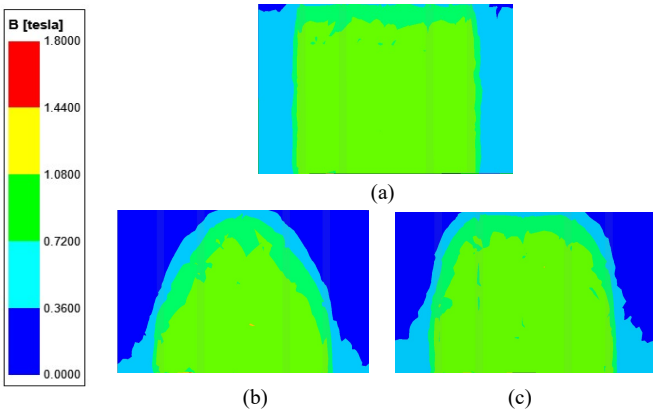

Fig. 3. The magnetic flux density distribution of half air gap of 20P18S motor. (a) Original Model. (b) Sine Model. (c) Sine+3rd Model.

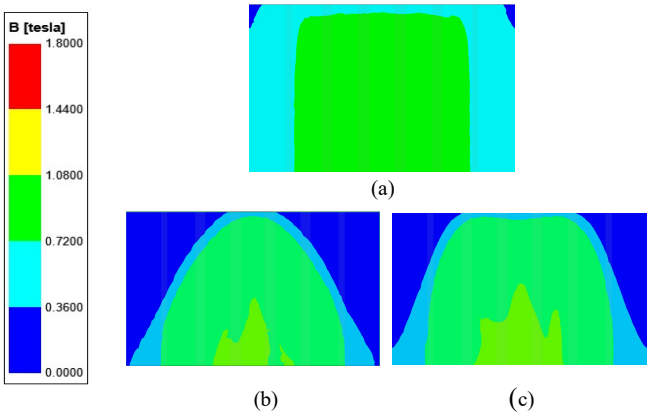

Fig. 4. The magnetic flux density distribution of half air gap of 16P18S motor. (a) Original Mode. (b) Sine Model. (c)Sine+3rd Model.

At the rated speed, the no-load phase electromotive force of the motor is Fourier decomposed. It can be seen from Fig. 5 that the fundamental amplitude of the original model, Sine model and Sine+3rd model of the 20P18S motor is 4.07 V, 4.08 V and 4.71 V, respectively. The fundamental amplitude of the Sine+3rd model is about 11.55 % of the Sine model. The fundamental amplitudes of 16P18S motor original model, Sine model and Sine+3rd model are 3.71 V, 3.72 V and 4.28 V respectively. The fundamental amplitude of Sine+3rd model is 11.51 % of the Sine model.

In reference [14], the torque ripple calculation formula is

$$T_{ripple}=\frac{T_{\max}-T_{\min}}{T_{\max}+T_{\min}}\times 100\% \tag{15}$$

where T_{max} and T_{min} are the maximum and minimum output torque.

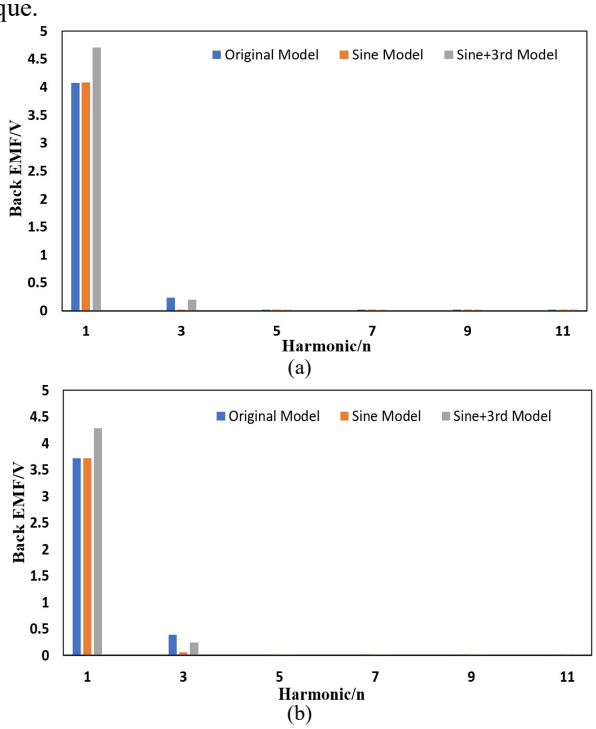

Fig. 5. Harmonic spectrum of no-load back EMF. (a)20P18S. (b) 16P18S.

Fig. 6 is the torque waveform comparison diagram of the three models. Table II and Table III show the output torque characteristics of the two motors.

The average output torque of the original model of the 20P18S motor is 14.5 N·m, and the torque ripple is 1.23 %. After sinusoidal shaping, the torque ripple is reduced to 0.43 %, which is 35 % of the original model torque ripple. However, the average output torque dropped significantly to 11.1 N·m, 76.5 % of the original model average output torque. After the third harmonic shaping is injected, the average output torque is 13.3N·m, which is 91.7 % of the original average output torque, which is 12 % higher than that of the Sine model, and the influence is obviously reduced. The torque ripple is 0.48 %, which is 39 % of the original model torque ripple, and the torque ripple is slightly higher than that of the Sine model.

The average output torque of the original model of the 16P18S motor is 6.7 N·m, and the torque ripple is 1.2 %. After sinusoidal shaping, the torque ripple is reduced to 0.46 %, which is 38.3 % of the original model torque ripple. However, the average output torque will also be greatly reduced to 5.17 N·m, which is 77.1 % of the original model average output torque. After the third harmonic shaping is injected, the average output torque is 6.06N·m, 90.5 % of the original model average output torque, 11.72 % higher than the Sine model, and the influence is significantly reduced. The torque ripple is 0.48 %, 40 % of the original model torque ripple, which is slightly higher than the Sine model torque ripple.

At the same time, from the comparison of the output torque characteristics of the two motors, it can be seen that compared with the original model, the Sine model and the Sine+3rd model not only reduce the torque ripple, but also improve the utilization of permanent magnets(Ratio of rated power of motor to total volume of permanent magnet). The utilization of permanent magnets of the two motors increased by 11.9 % and 12.1 %, respectively.

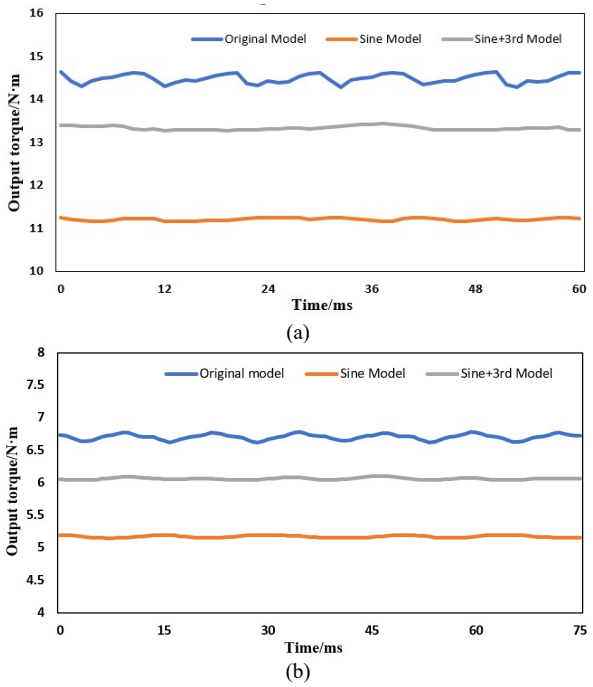

Fig. 6. Comparison diagram of torque waveform. (a) 20P18S. (b) 16P18S.

TABLE II
COMPARISON OF TORQUE CHARACTERISTICS OF THREE MODELS OF 20P18S MOTOR

	Original model	Sine model	Sine+3rd model
Output torque/(N·m)	14.5	11.1	13.3
Torque ripple/(%)	1.23	0.43	0.48
Permanent magnet volume /mm^3	54.4	34.6	42.2
Permanent magnet usage efficiency /(N·m·(mm^3)$^{-1}$)	0.27	0.32	0.32

TABLE III
COMPARISON OF TORQUE CHARACTERISTICS OF THREE MODELS OF 16P18S MOTOR

	Original model	Sine model	Sine+3rd model
Output torque/(N·m)	6.7	5.17	6.06
Torque ripple/(%)	1.2	0.46	0.48
Permanent magnet volume/mm^3	34.4	21.9	26.7
Permanent magnet usage efficiency /(N·m·(mm^3)$^{-1}$)	0.19	0.23	0.23

V. SEGMENTED DESIGN OF PERMANENT MAGNET

The permanent magnet sinusoidal plus third harmonic shaping method analyzed above can optimize the torque characteristics of the motor, but in practical applications, the processing requirements for permanent magnets are very high, which increases the manufacturing cost of the motor. In order to solve this problem, this section analyzes the method of permanent magnet segmentation.

Compared with the complex structure, the fabrication process of rectangular permanent magnet is relatively simple and the cost is low. Therefore, multiple rectangular permanent

magnets with the same thickness, the same axial length and different width can be spliced together to approximate the shape of the desired permanent magnet, as shown in Fig. 5.

In Fig.7 (a) and Fig.7 (b), the segmented of Sine model and the permanent magnet segmented of Sine+3rd model are respectively shown. In theory, the more segments of the permanent magnet, the higher the accuracy of the approximate equivalent, but it will also increase the manufacturing cost. In this paper, the sine shaping is divided into 5 segments along the axial length, and the width of each segment is the average of the maximum width and the minimum width of this segment. Since the shape of the Sine+3rd model is relatively more complex, the permanent magnet is divided into 9 sections to better approximate the shape of the two peaks.

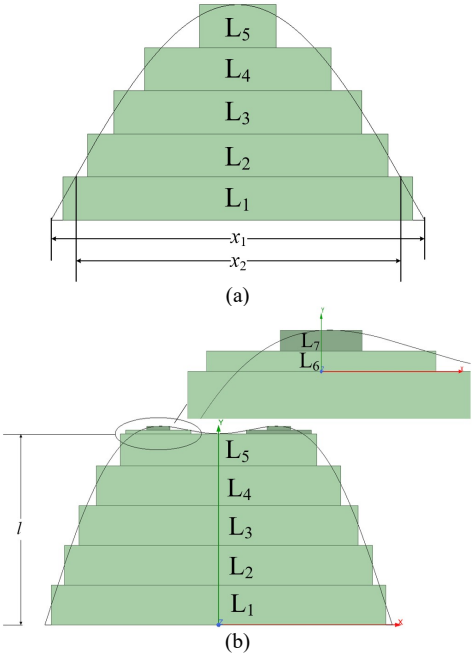

Fig. 7. Schematic diagram of permanent magnet segments. (a) Segmented of Sine model. (b) Segmented of Sine+3rd model.

The segmentation method of the sine model is to divide the permanent magnet into five segments along the axial length, and the width of each segment is the average value of the original sine curve in this segment. For example, the width expression of the L_1 segment is

$$(x_1+x_2)/2 \tag{16}$$

The segmentation processing method of the sine plus third harmonic model is that the axial distance to the concave point of the function curve is calculated by the formula, that is, the length of l, and then the permanent magnet of this part is segmented according to the processing method of sine segmentation. Finally, the protruding part of the model is divided into two segments according to the axial length, and the symmetry axis is made at the peak of the function, which is also segmented according to the processing method of the sinusoidal model.

The output torque waveforms of the permanent magnets of the two motors after sectional shaping are shown in Fig.8 The segmented of Sine model average output torque of the 20P18S motor is 11.6 N·m, and the torque ripple is 0.51 %. The average

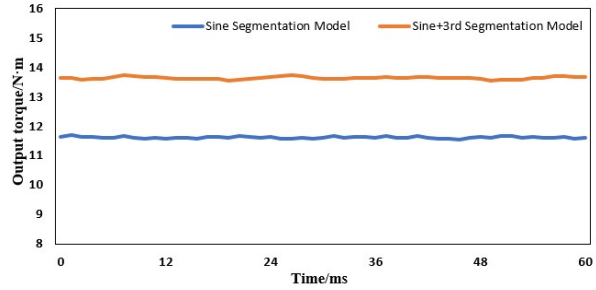

(a) 20P18S

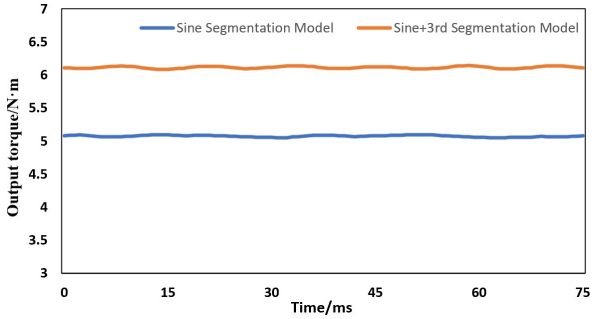

(b) 16P18S

Fig. 8. Comparison diagram of sectional torque waveform of permanent magnet.

TABLE IV
COMPARISON OF TORQUE CHARACTERISTICS OF PERMANENT MAGNET MODELS WITH DIFFERENT SHAPES FOR 20P18S MOTOR

Magnet shape	Output torque/(N·m)	Torque ripple/(%)
Original model	14.5	1.23
Sine model	11.1	0.43
Sine+3rd model	13.3	0.48
Segmented of Sine model	11.6	0.52
Segmented of Sine+3rd model	13.6	0.54

TABLE V
COMPARISON OF TORQUE CHARACTERISTICS OF PERMANENT MAGNET MODELS WITH DIFFERENT SHAPES FOR 16P18S MOTOR

Magnet shape	Output torque/(N·m)	Torque ripple/(%)
Original model	6.7	1.2
Sine model	5.17	0.46
Sine+3rd model	6.06	0.48
Segmented of Sine model	5.18	0.52
Segmented of Sine+3rd model	6.14	0.55

output torque is 13.6 N·m and the torque ripple is 0.54 % after segmented of Sine+3rd model. The segmented of Sine model average output torque of the 16P18S motor is 5.18 N·m, and the torque ripple is 0.48 %. The average output torque is 6.11 N·m and the torque ripple is 0.51 % after segmented of Sine+3rd model.

The output torque characteristics of each permanent magnet structure of the two motors are listed in Table IV and Table V. After the permanent magnet is segmented, the average output torque of the two structures is slightly improved. Because the segmented structure of the Sine+3rd model is more complex and the number of segments is more, the torque ripple changes little, increasing by 0.06 % and 0.07 %. The average output

torque is 93.8 % and 92 % of the original model.

VI. Conclusion

In this paper, a method of permanent magnet axial section shaping is discussed to suppress the torque ripple of surface-mounted permanent magnet synchronous motor. The third harmonic is injected into the sinusoidal shaping permanent magnet to improve the average output torque of the motor. Firstly, the optimal shape of permanent magnet is deduced from the calculation formula of back electromotive force and electromagnetic torque of permanent magnet motor. After that, through the finite element calculation of two surface-mounted permanent magnet synchronous motors, it is verified that after the third harmonic injection, the average output torque is increased by 12 % and 11.72 % respectively compared with the sinusoidal shaping, and the torque ripple is decreased by 61 % and 60 % respectively compared with the initial model, and the utilization rate of permanent magnets is increased by 11.9 % and 12.1 % respectively. While suppressing the torque ripple of the motor, it can also improve the utilization rate of permanent magnets and improve the economy of motor manufacturing. Finally, a method of reducing the manufacturing cost of permanent magnets by segmenting permanent magnets is discussed. The results show that the suppression effect of torque ripple after segmented of Sine+3rd model is almost the same as that of sinusoidal segmentation. The torque ripple of the two motors is reduced by 56 % and 54 % respectively compared with the initial model, and has little effect on the average output torque. This method can take into account the economy of motor manufacturing and the output torque characteristics of the motor.

References

[1] H. Mirahki, M. Ebrahimi, and B. Fahimi, "Asymmetrical Magnet Shape Optimization Based on S-C Mapping for Torque Profile Mitigation in Unidirectional Application of SPMS Machine," *IEEE Transactions on Transportation Electrification*, vol. 5, no. 3, pp. 630-637, Apr. 2019.

[2] M. Polat A. Yildiz, and R. Akinci, "Performance Analysis and Reduction of Torque Ripple of Axial Flux Permanet Magnet Synchronous Motor Manufactured for Electric Vehicles," *IEEE transactions on Magnetics*, vol. 57, no. 7, pp. 940-948, Aug. 2021.

[3] A. Ramezani, M. Ghiasi, and M. Dehghani *et al*, "Reduction of Ripple Toothed Torque in the Internal Permanent Magnet Eletric Motor by Creating Optimal Combination of Holes in the Rotor Surface Considering Harmonic Effects," *IEEE Access*, vol. 8, no. 12, pp. 215107-215124, Dec. 2020.

[4] V. S. Sempere, A. S. Gomez, and M. B. Payan *et al*, "Optimisation of Magnet Shape for Cogging Torque Reduction in Axial-flux Permanent-magnet Motors," *IEEE Access*, vol. 36 no. 4, pp. 2825-2838, May. 2021.

[5] C. Feng, L. P. Xin, and P. Y. Long, "Magnet Shape Optimization of Surface-mounted Permanent-magnet Motors to Reduce Harmonic Iron Losses," *IEEE Transactions on Magnetics*, vol. 52, no. 7, pp. 1582-1585, Oct. 2016.

[6] Z. H. Ming, Y. S. Bo, and S. Feng, "Harmonic Suppression and Torque Ripple Reduction of a High-speed Permanent Magnet Spindle Motor," *IEEE Access*, vol. 9, no. 4, pp. 51695-51702, Mar. 2021.

[7] H. Y. Wei, "Research on Torque Ripple Optimization of Built-in Permanent Magnet Synchronous Motor", Shenyang University of Technology, Shenyang, Jun. 2021.

[8] Z. W. Liang, S. H. Zhen, and C. W. Ping, et al, "Optimal Design and Experimental Test of a SPM Motor with Cost-effective Magnet Utilization to Suppress Torque Pulsations," *IEEE Transactions on Magnetics*, vol. 54, no. 11, pp. 876-880, Apr. 2018.

[9] J. L. Bing, L. Z. Gao, and Q. R. Hai, "Investigation of a Surface PM Machine with Segmented-eccentric Magnet Poles," *IEEE Transactions on Applied Superconductivity*, vol. 28, no. 3, pp. 1251-1255, May. 2018.

[10] H. M. Wang, S. Liu, and S. Wu, "Optimal Design of Permanent Structure to Reduce Unbalanced Magnetic Pull in Surface-mounted Permanent-magnet Motors," *IEEE Access*, vol. 8, no. 5, pp. 77811-77819, Oct. 2020.

[11] Y. Li, J. B. Zhou, and Y. P. Lu, "Optimum Design of Magnet Shape in Permanent-magnet Synchronous Motor," *IEEE Transactions on Magnetics*, vol. 39, no. 6, pp. 3523-3526, Jun. 2003.

[12] Chen Shikun. *Design of motor*. Beijing, Machinery Industry Press, 2000, pp. 9-10.

[13] H. S. Dao, Z. J. Ping, and J. Gao, et al, "Optimization the Electromagnetic Torque Ripple of Permanent Magnet Synchronous Motor," in *Proc. of International Conference on Electrical and Control Engineering*, Wuhan, China, pp. 3969-3972, Oct. 2010.

[14] J. C. Tan, *Permanent magnet brushless DC motor technology*. Beijing, Machinery Industry Press, 2018, pp. 177.

Shengnan Wu (M'18) was born in Yingkou, China. She received the B.S., M.S., and Ph.D. degrees in electrical engineering from the Shenyang University of Technology, Shenyang, China, in 2008, 2011, and 2017, respectively.

She is currently a Postdoctoral Research Assistant in electrical engineering with Shenyang University of Technology. Her research interests include electromagnetic design and multiphysical field simulation and analysis of permanent magnet machines.

Qifeng Zhao was born in Dandong, China. He received his bachelor's degree in electrical engineering from Shenyang University of technology in Shenyang, China in 2020. Currently, he is studying for a master's degree in electrical engineering at Shenyang University of technology in China.

His main research direction is high performance permanent magnet motor and its control, optimization design.

Wenming Tong (M'18) was born in Dandong, China. He received the B.S. and Ph.D. degrees in electrical engineering from the Shenyang University of Technology, Shenyang, China, in 2007 and 2012, respectively. He is currently an Associate Professor with the National Engineering Research Center for Rare Earth Permanent Magnet Machines, Shenyang University of Technology.

His major research interests include the design, analysis, and control of high-speed and low-speed direct drive permanent magnet machines, axial flux permanent magnet machines, hybrid excitation machines, and high-performance machines with new types of soft magnetic materials.